Optics Communications 307 (2013) 32–38

Contents lists available at SciVerse ScienceDirect

Optics Communications

journal homepage: www.elsevier.com/locate/optcom

Intensity-dependent dynamics of the correlated electrons in molecular double ionization driven by mid-infrared laser pulses ☆

Qingbin Tang, Dongling Zhang, Molin Liu, Yang Gao, Benhai Yu *

College of Physics and Electronic Engineering, Xinyang Normal University, Xinyang 464000 China

ARTICLE INFO

Article history:
Received 22 January 2013
Received in revised form
28 May 2013
Accepted 30 May 2013
Available online 14 June 2013

Keywords:
Nonsequential double ionization
Recollision threshold
Electron correlation

ABSTRACT

With the three-dimensional classical ensemble model, we have investigated the complex electron correlations in N_2 double ionization by the mid-infrared laser pulses over a wide range of laser intensities. Our numerical results show that the correlated longitudinal electron momentum spectra exhibit rich correlated patterns with the increase of the laser intensity. At the low and high laser intensities, the correlated electron momentum spectra display an obvious finger-like structure, while at the moderate laser intensity the finger-like structure is not observed and there is a certain contribution from the back-to-back emission. By back-analyzing the classical trajectories, the subcycle dynamics of the molecular double ionization in the long-wavelength regime are revealed and the complex electron correlations are explained.

1. Introduction

The study of the electron correlations has been a hot topic in the past decades because it is the underlying mechanism for many phenomena in strong field laser-matter interactions. Different from the sequential double ionization (SDI) [1,2], where the both electrons ionize mainly due to their individual interaction with the laser field, non-sequential double ionization (NSDI) of atoms and molecules represents one of the most prominent and intriguing examples of a correlated electron–electron process driven by the external laser field. In particular, the NSDI of the atoms and molecules provides us with an effective way to study and control the electron dynamics in an external laser field as the electron–electron correlation plays a crucial role in the NSDI process [3,4] and it has drawn a great number of experimental and theoretical studies [5–21]. The differential measurements of the recoil ion and emitted electron momenta [3,7,11] provide strong evidences that the rescattering mechanism [22,23] is dominantly responsible for the NSDI process. According to this recollision scenario, an electron is ionized by the laser field. Then it is driven by the oscillating electric field and returns to the parent ion as the electric field reverses its direction, recolliding with the ion inelastically and leading to the second electron freed directly in an (e. 2e) process or excited with subsequent field ionization (RESI) [7]. This rescattering mechanism is also responsible for the high-order harmonic generation [24–27] and high-order above threshold ionization [28]. The physical mechanism of NSDI has been profoundly investigated by means of the correlated electron momentum distributions [3,12,29]. Based on the general recollision scenario [22], more detailed dynamics processes are proposed to explain the novel characteristics of correlated electron momentum distributions in NSDI [7,12,18,19,30].

The investigations [12,18,31–36] have shown that the double ionization dynamics in the strong field exhibit rich correlated patterns with the change of the laser intensity. The finger-like structure in the correlated longitudinal (in the direction parallel to the laser polarization) momentum distribution from NSDI of helium at the moderate laser intensity indicates backscattering at nucleus upon recollision [12]. At the high intensity, Rudenko et al. observed a pronounced V-like shape of the correlated electrons momentum distribution [31], which is interpreted as a consequence of Coulomb repulsion and the typical (e, 2e) kinematics. Theoretical interpretation of these finger-like structures has advanced by many theoretical calculations [18,32–34]. With the help of classical trajectory diagnosis, the distinct roles of the nuclear Coulomb attraction and the final-state electron repulsion (at the moderate laser intensity) and the asymmetric energy-sharing recollision (at the high laser intensity) in forming of the finger-like structure have been identified for atom NSDI [18,32,33], respectively. Recently, the line-like distribution parallel to the diagonal $P_{\|e1} = P_{\|e2}$ in the correlated momentum spectra is found for argon NSDI at the low laser intensity and the classical analysis illustrates that the ionization time difference between the two

* Corresponding author.
E-mail address: hnyubenhai@163.com (B. Yu).

0030-4018/$ - see front matter © 2013 The Authors. Published by Elsevier B.V. All rights reserved.
http://dx.doi.org/10.1016/j.optcom.2013.05.054

electrons is crucial for the emergence of the line-like distribution [35]. However, the finger-like structure has never been observed for NSDI of Ne [9,37], which indicates that the structure of the target decisively influences the electron momentum correlation pattern. Peculiarly, up to now, the structure in the correlated electrons longitudinal momentum distribution from molecular NSDI has not reported. Furthermore, the dynamical electron correlations in the strong-field NSDI exhibit strong dependence on the laser wavelengths [38–40]. For instance, in Refs. [39,40], it has been shown that the shape of longitudinal momentum distributions of the doubly charged ion for atoms and molecules is a double-hump structure in the long-wavelength regime, different from the single-hump structure in the near-infrared (NIR) regime. This double-hump becomes more pronounced as the wavelength further increases.

Compared with the atomic case, the structure of diatomic molecules is more complicated due to additional molecular freedom [41]. Furthermore, due to the huge computational demand of describing the many-body interaction in the long-wavelength laser field, the wavelengths of the laser pulse in those previous studies are mainly in the short-wavelength region ($\lambda \leq 0.8$ μm) and the complex electron dynamics which is crucial for molecular double ionization (DI) in the long-wavelength regime is not detailedly explored. In this work, we investigate the correlated electron dynamics in N_2 DI by the 1300-nm laser pulses over a wide range of laser intensities from 4×10^{13} W/cm^2 to 2×10^{15} W/cm^2 with the three-dimensional (3D) classical ensemble model [19]. The numerical result shows that the two-electron momentum distributions, strongly dependent on the laser intensity, exhibit rich correlated patterns. At the low and high laser intensities, the finger-like structures in the correlated momentum distribution are obvious, which are similar to the previous experimental results for atoms [31,35]. Through back analysis of the trajectories, the distinct roles of the ionization time differences between the two electrons and the asymmetric energy-sharing in forming of the finger-like structure are identified for molecular NSDI events provoked by recollision. But at the moderate laser intensity, the finger-like structure is not presented and there is a certain contribution from the back-to-back emission. By back-analyzing the classical trajectories, the subcycle dynamics of the molecular double ionization in the long-wavelength regime are revealed and the complex electron correlations are explained. When the laser intensity increases to or above 1×10^{15} W/cm^2, the DI is dominated by a collisionless SDI.

2. The classical ensemble model

Here we employ the classical model introduced by Eberly et al. to investigate NSDI of N_2 [19]. This classical model has been successful in understanding of NSDI before [18,19,32,42–44]. The evolution of the system in this model is determined by the classical equation of motion. (Atomic units are used throughout the paper if not stated otherwise.) $d^2\mathbf{r}_i/dt^2 = -\mathbf{E}(t) - \nabla[V_{ne}(\mathbf{r}_i) + V_{ee}(\mathbf{r}_1,\mathbf{r}_2)]$, where the subscript i is the label of the two different electrons and $\mathbf{E}(t)$ is the linearly polarized electric field. The nucleus–electron and electron–electron interaction are represented by a 3D soft-Coulomb potential $V_{ne} = -1/\sqrt{(\mathbf{r}_1+R/2)^2+a^2} - 1/\sqrt{(\mathbf{r}_1-R/2)^2+a^2} - 1/\sqrt{(\mathbf{r}_2+R/2)^2+a^2} - 1/\sqrt{(\mathbf{r}_2-R/2)^2+a^2}$ and $V_{ee} = 1/\sqrt{(\mathbf{r}_1-\mathbf{r}_2)^2+b^2}$, respectively. To obtain the initial value, the ensemble is populated starting from a classically allowed position for the N_2 ground state energy of −1.67 a.u. The available kinetic energy is distributed between the electrons randomly. Then the electrons are allowed to evolve a sufficient long time in the absence of the laser field to obtain stable position and momentum distributions [6,21,43]. To avoid autoionization and ensure stability, we set the screening parameter a and b to be 1.15 a.u. and 0.05 a.u., respectively. In present calculations, the internuclear distance R is set to be 2.0 a.u. corresponding to N_2 molecule. The electric field $\mathbf{E}(t)$ is a linearly polarized laser pulse with a polarization direction along the z-axis. The pulses are trapezoidal shape with two-cycle turn on, six cycles at full strength, and two-cycle turn off. After the laser pulse is turned off, we define double ionization if both electrons have positive energy.

Theoretically, an accurate description of strong field DI needs full quantum theory. But so far, because of the enormous computational demand, full-dimensional solution of the time dependent schrödinger equation has only been performed on NSDI of helium by 400 nm laser pulses [45]. In the long-wavelength regime, it seems impossible to extend this quantum-mechanical calculation to DI that involves two correlated electrons in the foreseeable future. Furthermore, lots of studies have shown that in strong field DI, the classical model can catch most of the features in double ionization [2,10,18,19,32,46,47]. This may be due to the high intensity of the laser field where the quantum effect is weak, and thus the results of strong field DI from the classical calculation are reliable even though the quantum effects cannot be captured. So, in this work, we employ the classical model to provide intuitive insight into the complex electron dynamics in strong field DI. Moreover, for molecules, with the quantum theory it has been shown that the two-center interference and the orbital geometry play important roles in NSDI [41]. Of course, these quantum effects could not be captured by classical models. Investigations on these effects must resort to quantum model [41]. In this paper, we focus on the intensity-dependence dynamics of correlated electrons involved in molecule NSDI at the long-wavelength regime. For these issues, the classical model has been proved to be valid [39,47].

3. Results and discussions

In Fig. 1, the DI yields are plotted with respect to the laser intensities from 4×10^{13} W/cm^2 to 2×10^{15} W/cm^2. In consistency with the previous experimental results [41], the knee structure is clearly seen in the curve, which implies non-sequential (NS) ionization channel dominating molecule DI in the middle-infrared (MIR) regime. According to the numerical results, the curve can be divided into two parts (the vertical green dot line shows the separate location): the NSDI (from 4×10^{13} W/cm^2 to 1×10^{15} W/cm^2) and the SDI (from 1×10^{15} W/cm^2 to 2×10^{15} W/cm^2) intensity region, where the DI is dominated by a recollision and a collisionless double ionization, respectively. In this paper, we concentrate on the intensity range where NS dominates DI. A simple estimation of the intensity threshold is given by $3.17U_p = |I_{P_2}|$, which gives 6×10^{13} W/cm^2. In the low-intensity regime when the laser intensity is less than the threshold, the delayed ejection pathway plays an important role while the recollision ionization (RCI, where the second electron ionizes directly by the recollision of the first electron) mechanism dominates NSDI when the laser intensity exceeds the recollision threshold. Back-analysis of classical trajectories indicates that the dominant mechanisms in various intensity regimes are widely divergent and which will be shown later.

Tracing back the temporal evolution history of DI trajectories allows us to unveil the microcosmic dynamics of molecular DI. Such a classical trajectory perspective could provide an intuitive way to understand the complex dynamics involved in molecular DI. The typical trajectories responsible for molecular DI are plotted in Fig. 2 as presented in energy versus time. Below the recollision threshold intensity, back analysis reveals that there exist two dominant

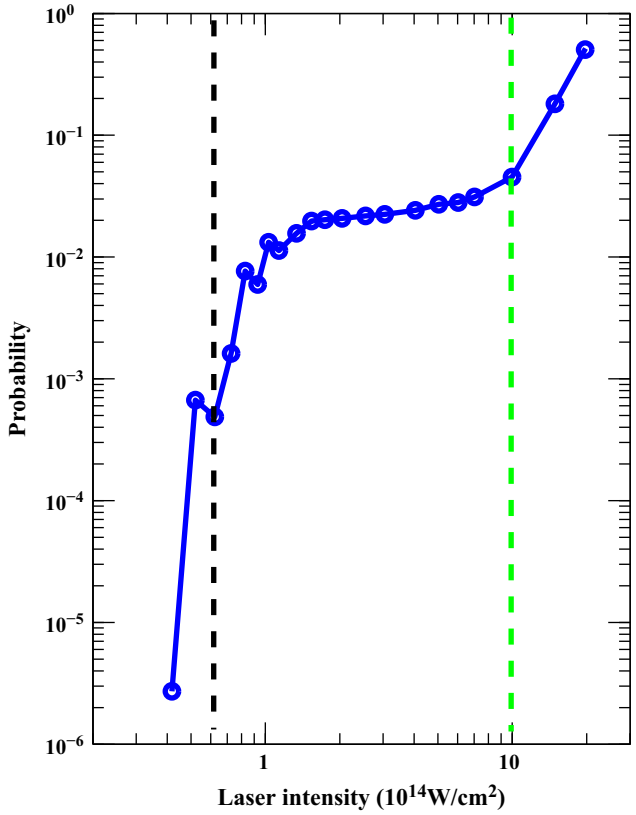

Fig. 1. Double ionization probabilities as a function of the laser intensity. The laser wavelength is 1300 nm. 6×10^{13} W/cm^2 is the threshold intensity as indicated by the vertical black dot line (the left dot line). (For interpretation of the references to color in this figure caption, the reader is referred to the web version of this article.)

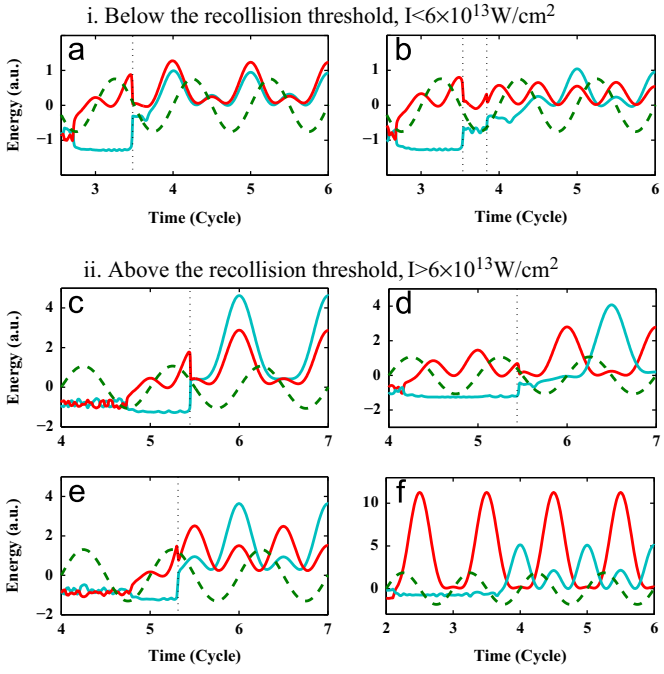

Fig. 2. Typical energy evolution of the electron pair in a different intensity regime. Vertical dashed lines indicate the moment when collision between electrons emerge.

processes responsible for emitting two electrons, single- and multiple-recollision-induced correlated emission, as shown in Fig. 2(a) and (b), respectively. For the both responsible DI processes, by inspecting the DI trajectories, we find that the most likely scenario for this intensity regime is the production of a doubly excited state (DES) [see Fig. 2(a) and (b)] after the recollision, which is consistent with the case at the NIR regime where there exists a short-lived DES after the recollision [35,47]. For the low laser intensity, the maximal recolliding energy of the return electron is insufficient to directly ionize the inner electron. Thus, after recollision, the two electrons undergo a time-delayed field-assisted ionization of the excited state. Fig. 2(a) shows that the time delay between the recollision and DI is about 1/4T [where the T is laser cycle, 1T~4.3 fs], which implies that the two electrons escape into the same hemisphere [19]. In Fig. 2(b), the semiliberated electron returns to the core repeatedly. During each return the efficiency of the energy transfer rests on the relative motional phase between the two electrons [48]. Fig. 2(b) shows that after the final recollision, the bound electron undergoes a time-delayed [~T/2], which results in the two electrons which may be able to escape into the opposite hemisphere [19,49]. Our statistics show that below the recollision threshold intensity the former DI pathway dominates NSDI at the long-wavelength regime. For instance, when $I = 5 \times 10^{13}$ W/cm^2 the proportions of this DI pathway are above 70% of the total DI events and thus the electron pairs from NSDI are more likely to escape into the same hemisphere [see Fig. 3(a)].

When the instantaneous laser field is above the recollision threshold intensity we observe three types of trajectories [except for SDI (Fig. 2(f))] indicated by Fig. 2(c)–(e) represent the dominant processes of NSDI from 6×10^{13} W/cm^2 to 1×10^{15} W/cm^2. The RCI [see Fig. 2(c) and (e)] and RESI [see Fig. 2(d)] are responsible processes for emitting both electrons. Fig. 2(c)–(e) shows that there exists only one time recollision in the molecular DI process, which is difference from the case in the low intensity regime. Fig. 2(c) and (d) shows that the recollisions occur in the time just before the zero crossing of the field. It is consistent with the prediction of the simple-man model [22]. While, we observe a surprising RCI pathway [see Fig. 2(e)], the recollision occurs in the moment near the extreme of the laser field and the bound electron is ionized quickly through collision with the returned electron. Our statistics suggests that the contribution of the RCI mechanism increases and the RESI mechanism decreases as the laser intensity increases. However, when the laser intensity further increases the contribution of the RCI mechanism will decrease and the contribution of the SDI mechanism increases with the laser intensity increasing. We define SDI as the pathway where there is no recollision and both electrons ionize mainly due to their individual interaction with the laser field. When the laser intensity is higher, i.e., at or above 1×10^{15} W/cm^2, DI is dominated by a collisionless SDI in which the typical trajectory is represented by Fig. 2(f).

The correlated electron longitudinal momentum spectrum can provide more detailed insight into the electron dynamics, thus in Fig. 3 we illustrate the correlated electron momentum spectra in the direction parallel to the laser field for different laser intensities when the molecular axis is parallel to the laser polarization, P_{z1}, P_{z2} represent the momentum components of the two electrons parallel to the laser field direction. Fig. 3 shows that in the long-wavelength regime the correlated electron momentum spectra exhibit rich correlated patterns with the increase of the laser intensity. In the NSDI intensity region [see Fig. 3(a)–(e)], the electron pairs from NSDI are more likely to emit into the same hemispheres. In particular, at the low laser intensity [see Fig. 3(a)], the correlated electrons momentum distribution exhibits a clear finger-like structure. This is similar to the correlated momentum distribution of argon NSDI at low laser intensity presented in a recent study [35], where the line-like structure is found below the recollision threshold intensity. At the moderate laser intensity, the finger-like structure is not presented [see Fig. 3(b) and (c)] and while at the high laser intensity [see Fig. 3(e)], the finger-like

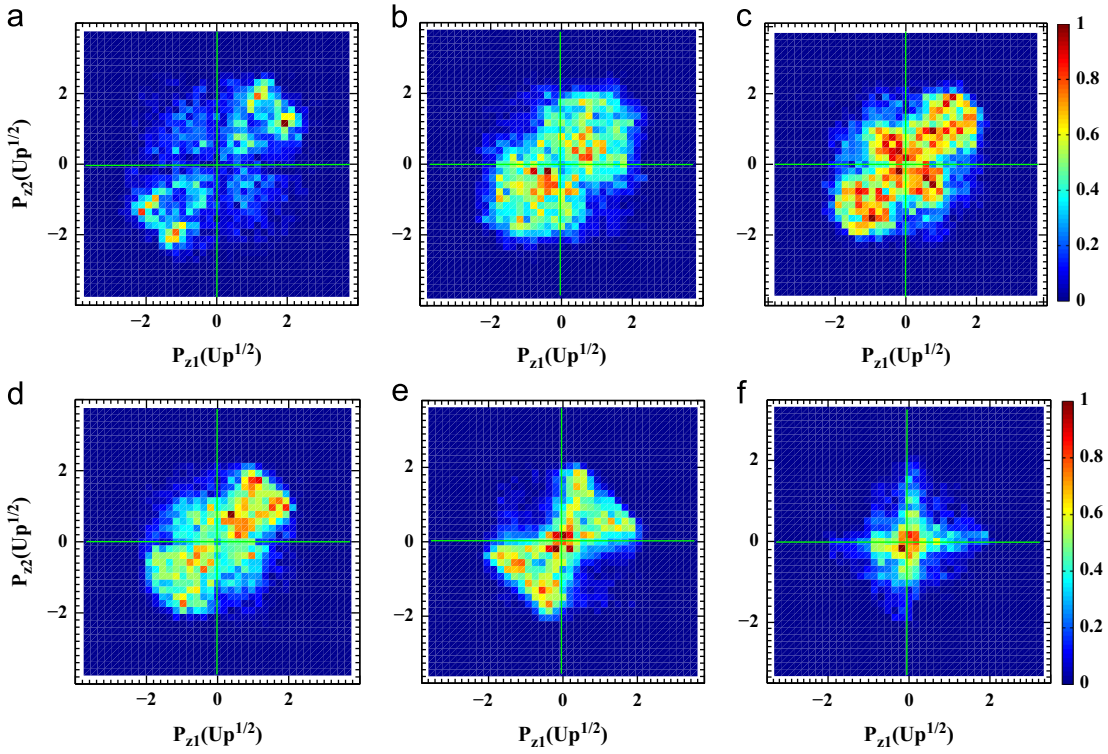

Fig. 3. The correlated electron momentum distributions in the direction parallel to the laser polarization for DI of N_2 molecules. The laser intensities are 0.5×10^{14} W/cm^2 (a), 1×10^{14} W/cm^2 (b), 1.5×10^{14} W/cm^2 (c), 2×10^{14} W/cm^2 (d), 4×10^{14} W/cm^2 (e), 10×10^{14} W/cm^2 (f). In (a) the ensemble are 7 millions, in (b)–(d) the ensemble are 1 million and in (e) and (f) the ensemble are 0.5 million. In all plots, the events where DI occurs at the turn-on stage of the trapezoidal pulse are excluded.

structure in the correlated momentum distribution is obvious. In contrast to the result at the low laser intensity [see Fig. 3(a)], a cluster of distribution around zero momentum is clearly seen [see Fig. 3(e)]. Back analysis reveals that these events correspond to the trajectories where DIs occur through a collisionless SDI.

By tracing the classical DI trajectories we can find that in the low laser intensity the ionization time differences between the two electrons contribute to the finger-like structure in the correlated longitudinal electron momentum. To illustrate this point, we inspect the correlated momentum plots for various $\Delta t=t_2^i-t_1^i$. The results are presented in Fig. 4. For each DI event i the ionization times t_1^i and t_2^i of the electrons 1 and 2, respectively, are defined as the instant when the energy of the electron becomes positive for the first time after the recollision, where the energy of each electron contains the kinetic energy, potential energy of the electron–ion interaction and half electron–electron repulsion. In Fig. 4(a) and (b), we have segregated the trajectories shown in Fig. 3(a) according to the ionization time difference of the two electrons. Fig. 4(a) and (b) displays the correlated longitudinal electron momentum distributions of the trajectories where the ionization time difference Δt is smaller than $0.3T$ and larger than $0.5T$, respectively. It is clearly shown that the correlated longitudinal electron momentum distribution exhibits a finger-like structure and the electron pairs involved in NSDI mainly escape into the same hemispheres [see Fig. 4(a)] when the ionization time difference is smaller $0.3T$ (ionization within one half cycle). In contrast, the DI events are mainly clustered in the opposite hemispheres when the ionization time difference is larger than $0.5T$ [see Fig. 4(b)]. For the laser intensity $I=0.5\times10^{14}$ W/cm^2, our statistic shows that for the ionization time difference less than $0.3T$ the proportion of electron pairs is above 55% of the total DI events. And for the ionization time difference larger than $0.5T$ the proportion is about 30%. As a result, the DI events are mainly clustered in the first and third quadrants [see Fig. 3(a)]. According to the simple-man model [22], the momentum shift imposed onto the electron is equal to the instantaneous laser-field vector potential $P(t)=-A(t)$ (where t is the ionization time of the electron). Thus, for events resulting from ionization of both electrons within the same half cycle there exists a longitudinal momentum difference $\Delta P_z=P_{z2}-P_{z1}$ of the two electrons because of the released time difference between the two electrons from DES produced by recollision [35], which results in the finger-like structure of the correlated electrons momentum distributions. From what has been discussed above, we may draw the conclusion that in the long-wavelength regime, the finger-like structure in the longitudinal correlated electron momentum at the low laser intensity is a consequence of the ionization time difference of the two electrons.

In addition, Fig. 3(a) shows that there exists a little part of electrons with momentum greater than $2\sqrt{U_p}$ at low laser intensity. With the help of classical trajectory diagnosis, we find that the nuclear boomerang at recollision [6] is indeed important in their production at the long-wavelength regime. However, in the high intensity, almost no DI occurs through a nuclear boomerang and thus there is no electron with momentum greater than $2\sqrt{U_p}$.

At the high laser intensity, to explore the responsible dynamics for the finger-like structure in the long-wavelength regime, we take further advantage of the back analysis [48]. Tracing the classical DI trajectories allows us to easily determine the recollision time and the energy exchange during recollision. Here, the recollision time is defined to be the instant of the closest approach after the first departure of one electron from the core [19]. Fig. 5(a) displays the correlated electron momentum distributions in the direction parallel to the laser polarization for the events in Fig. 3(e), where the collisionless SDI are excluded. In Fig. 5(b) and (c), we have segregated the trajectories shown in Fig. 5(a) according to the energy difference of the two electrons at time $0.01T$ after

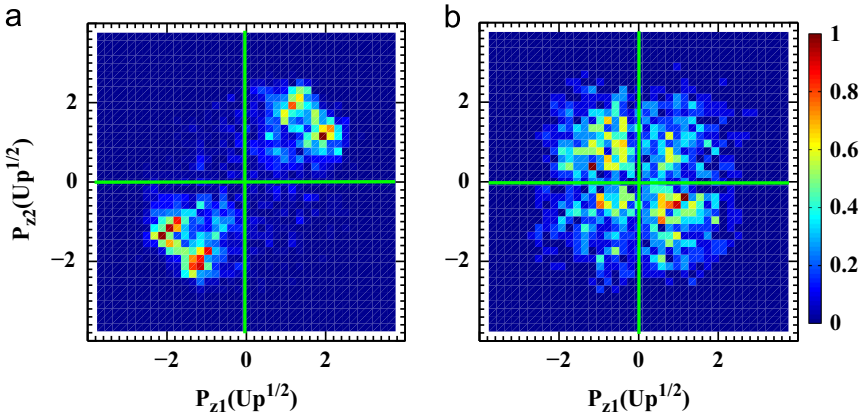

Fig. 4. Correlated longitudinal electron momentum distributions for the events in Fig. 3(a). The ionization time difference $\Delta t = t_2^i - t_1^i$ is (a) smaller than 0.3T and (b) larger than 0.5T.

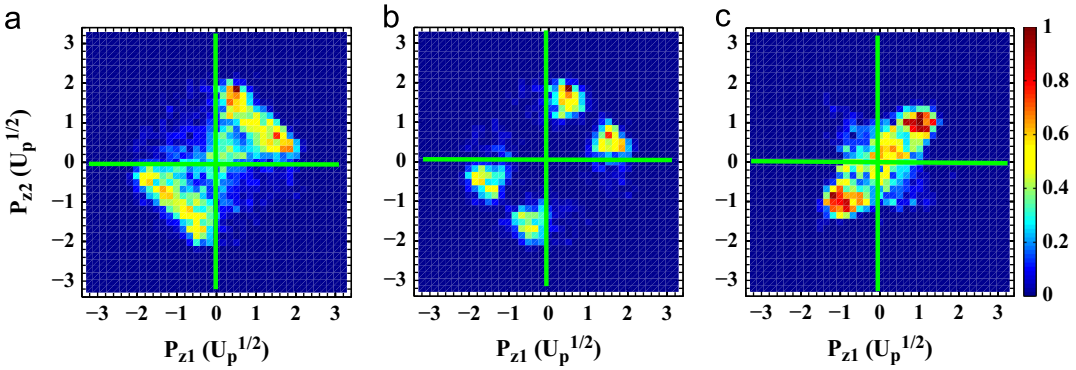

Fig. 5. (a) Correlated longitudinal electron momentum distributions for the events in Fig. 3(e), where the collisionless SDI are excluded. The energy difference at time 0.01T after recollision is (b) larger than 1 a.u. and (c) smaller than 1 a.u.

recollision. Fig. 5(b) and (c) displays the correlated longitudinal electron momentum distributions of the trajectories where the energy difference is larger and less than 1.0 a.u., respectively. It is clearly shown that the events are clustered on the main diagonal when the two electrons achieve similar energies at recollision [see Fig. 5(c)]. In contrast, the correlated electron momentum distribution exhibits distinct off-diagonal features when asymmetric energy sharing occurs [see Fig. 5(b)]. Based on these results, we can conclude that in the long-wavelength regime, the asymmetric energy sharing at recollision is the decisive reason for the finger-like structure in the longitudinal correlated electron momentum at the high laser intensity.

But at the moderate laser intensity, the finger-like structure is not observed [see Fig. 3(b), (c)]. Previous studies have illustrated that the finger-like structure is able to be reproduced for helium at relative moderate intensity when the realistic Coulomb potential or a softened potential with a smaller screening parameter is used [32,33]. Thus, we think that maybe because of the large soft parameter employed in our calculation, the finger-like structure is not observed at moderate intensity. Due to the huge computational demand of describing the many-body interaction in the long-wavelength laser field, the supposition has not been demonstrated in this paper. Additionally, we find that there is a certain contribution from the back-to-back emission. Our statistic shows that for the 1300-nm pulses the proportions of the electron pairs emitted into the opposite hemisphere are about 34%, 40%, and 33% for the laser intensities $I = 1 \times 10^{14}$ W/cm^2, 1.5×10^{14} W/cm^2, 2×10^{14} W/cm^2, respectively. This indicates that the yields of the anticorrelated electrons are not ignorable. So, at the moderate laser intensity, the correlated behavior is different from that in the NIR regime, where the yields of the anticorrelated electrons decrease continuously and then the double-hump structure of ion momentum spectra becomes more pronounced as the intensity increases [36]. When the laser intensity enters the higher intensity regime, more and more electron pairs from DI occur through sequential ionization pathway and emit into the region near the zero-momentum as the laser intensity increases [see Fig. 3 (e) and (f)].

In order to understand the microscopic dynamics process for the anticorrelated emissions at the moderate laser intensity, we take advantage of back analysis. By back-analysis classical trajectories we find that there exist a number of classical trajectories of the recollision that occur near the field maximum [see Fig. 2(e)] in the moderate laser intensity, which may be the responsible cause of the anticorrelated emissions. In Fig. 6, we have segregated the trajectories shown in Fig. 3(b)–(d) according to the recollision time. Fig. 6(d)–(f) displays the correlated longitudinal electron momentum distributions of the trajectories where the phase of the recollision times is 0.2T–0.3T and 0.7T–0.8T. It is clearly shown that the events are clustered on the opposite hemispheres when the recollisions occur near the field maximum. In contrast, the correlated electron momentum distribution shows that the electron pairs are more likely to emit into the same hemisphere when the recollisions occur near the zero-crossing of the laser field [see Fig. 6(a)–(c)]. For the former DI population, after recollision, the electron pairs emit into opposite directions because the laser field only provides a small drift momentum [7,43]. This process results in a certain proportion of the opposite electron pairs at the moderate laser intensity.

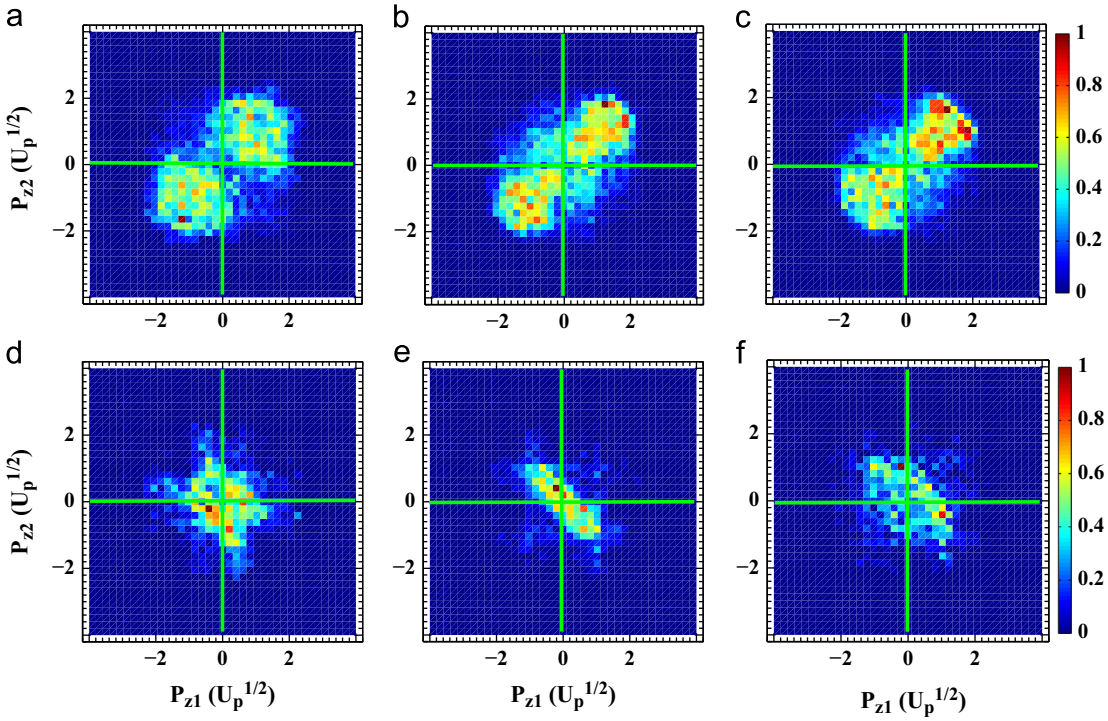

Fig. 6. Correlated longitudinal electron momentum distributions for the trajectories deduced from Fig. 3(b)–(d) by superimposing additional restrictions on our statistics according to different recollision times.

4. Summary

In summary, we have investigated the complex electron correlations in N_2 DI by the MIR laser pulses over a wide range of laser intensities. Our numerical results show that the correlated longitudinal electron momentum spectra exhibit rich correlated patterns with the increase of the laser intensity. At the low and high laser intensities, the correlated electron momentum spectra display an obvious finger-like structure, while at the moderate laser intensity such finger-like structure is not observed and there is a certain contribution from the back-to-back emission. Back analysis reveals that in the long-wavelength regime, the ionization time differences between the two electrons and the asymmetric energy sharing at recollision are the decisive reasons for the finger-like structure in the longitudinal correlated electron momentum at the low and high laser intensities, respectively. As a consequence, the finger-like structure in the correlated momentum spectrum from molecular NSDI depends on the laser intensity strongly.

Acknowledgments

This work was supported by the National Natural Science Foundation of China under Grant no. 11047145, the Science and Technology Project of Henan Province in China under Grant no. 112300410021, the Scientific Research Foundation of Education Department of Henan Province in China under Grant no. 2011B140018, 13A140774.

References

[1] A.N. Pfeiffer, C. Cirelli, M. Smolarski, R. Dörner, U. Keller, Nature Physics 7 (2011) 428.
[2] Y. Zhou, C. Huang, Q. Liao, P. Lu, Physical Review Letters 109 (2012) 053004.
[3] Th. Weber, H. Giessen, M. Weckenbrock, G. Urbasch, A. Staudte, L. Spielberger, O. Jagutzki, V. Mergel, M. Vollmer, R. Dörner, Nature (London) 405 (2000) 658.
[4] D.N. Fittinghoff, P.R. Bolton, B. Chang, K.C. Kulander, Physical Review Letters 69 (1992) 2642.
[5] B. Walker, B. Sheehy, L.F. Dimauro, P. Agostini, K.J. Schafer, K.C. Kulander, Physical Review Letters 73 (1994) 1227.
[6] Y. Zhou, Q. Liao, P. Lu, Physical Review A 80 (2009) 023412.
[7] B. Feuerstein, R. Moshammer, D. Fischer, A. Dorn, C.D. Schröter, J. Deipenwisch, J.R. Crespo López-Urrutia, C. Höhr, P. Neumayer, J. Ullrich, H. Rottke, C. Trump, M. Wittmann, G. Korn, W. Sandner, Physical Review Letters 87 (2001) 043003.
[8] Q. Liao, Y. Zhou, C. Huang, P. Lu, New Journal of Physics 14 (2012) 013001.
[9] M. Weckenbrock, D. Zeidler, A. Staudte, Th. Weber, M. Schöffler, M. Meckel, S. Kammer, M. Smolarski, O. Jagutzki, V.R. Bhardwaj, D.M. Rayner, D.M. Villeneuve, P.B. Corkum, R. Dörner, Physical Review Letters 92 (2004) 213002.
[10] Y. Zhou, C. Huang, P. Lu, Physical Review A 84 (2011) 023405.
[11] A. Rudenko, K. Zrost, B. Feuerstein, V.L.B. de Jesus, C.D. Schröter, R. Moshammer, J. Ullrich, Physical Review Letters 93 (2004) 253001.
[12] A. Staudte, C. Ruiz, M. Schöffler, S. Schössler, D. Zeidler, Th. Weber, M. Meckel, D.M. Villeneuve, P.B. Corkum, A. Becker, R. Dörner, Physical Review Letters 99 (2007) 263002.
[13] Y. Zhou, C. Huang, Q. Liao, W. Hong, P. Lu, Optics Letters 36 (2011) 2758.
[14] R. Kopold, W. Becker, H. Rottke, W. Sandner, Physical Review Letters 85 (2000) 3781.
[15] A. Becker, R. Dörner, R. Moshammer, Journal of Physics B 38 (2005) S753.
[16] Q. Liao, P. Lu, Physical Review A 82 (2010) 021403. (R).
[17] M. Lein, E.K.U. Gross, V. Engel, Physical Review Letters 85 (2000) 4707.
[18] Y. Zhou, Q. Liao, P. Lu, Physical Review A 82 (2010) 053402.
[19] S.L. Haan, L. Breen, A. Karim, J.H. Eberly, Physical Review Letters 97 (2006) 103008.
[20] Q. Liao, P. Lu, Q. Zhang, W. Hong, Z. Yang, Journal of Physics B 41 (2008) 125601.
[21] Y. Zhou, C. Huang, A.H. Tong, Q. Liao, P. Lu, Optics Express 19 (2011) 2301.
[22] P.B. Corkum, Physical Review Letters 71 (1993) 1994.
[23] K.J. Schafer, B. Yang, L.F. DiMauro, K.C. Kulander, Physical Review Letters 70 (1993) 1599.
[24] F. Krausz, M. Ivanov, Reviews of Modern Physics 81 (2009) 163.
[25] P. Lan, P. Lu, W. Cao, Y. Li, X. Wang, Physical Review A 76 (2007) 011402. (R).
[26] W. Cao, P. Lu, P. Lan, X. Wang, G. Yang, Physical Review A 74 (2006) 063821.
[27] P. Lan, P. Lu, F. Li, Y. Li, Z. Yang, Optics Express 16 (2008) 5868.
[28] W. Becker, F. Grasbon, D.B. Kopold, D.B. Miloševič, G.G. Paulus, H. Walther, Advances in Atomic Molecular and Optical Physics 48 (2002) 36.
[29] Y. Liu, S. Tschuch, A. Rudenko, M. Dürr, M. Siegel, U. Morgner, R. Moshammer, J. Ullrich, Physical Review Letters 101 (2008) 053001.
[30] B. Yu, D. Zhang, Y. Li, Q. Tang, Journal of Modern Optics 59 (2012) 679.
[31] A. Rudenko, V.L.B. deJesus, T. Ergler, K. Zrost, B. Feuerstein, C.D. Schroter, R. Moshammer, J. Ullrich, Physical Review Letters 99 (2007) 263003.
[32] S.L. Haan, J.S. Van Dyke, Z.S. Smith, Physical Review Letters 101 (2008) 113001.
[33] D. Ye, X. Liu, J. Liu, Physical Review Letters 101 (2008) 233003.
[34] A. Emmanouilidou, Physical Review A 78 (2008) 023411.
[35] N. Camus, B. Fischer, M. Kremer, V. Sharma, A. Rudenko, B. Bergues, M. Kübel, N.G. Johnson, M.F. Kling, T. Pfeifer, J. Ullrich, R. Moshammer, Physical Review Letters 108 (2012) 073003.

[36] A. Rudenko, Th. Ergler, K. Zrost, B. Feuerstein, V.L.B. de Jesus, C.D. Schröer, R. Moshammer, J. Ullrich, Physical Review A 78 (2008) 015403.
[37] R. Moshammer, J. Ullrich, B. Feuerstein, D. Fischer, A. Dorn, C.D. Schröter, J.R. Crespo López-Urrutia, C. Höhr, H. Rottke, C. Trump, M. Wittmann, G. Korn2, K. Hoffmann, W. Sandner, Journal of Physics B 36 (2003) L113.
[38] O. Herrwerth, A. Rudenko, M. Kremer, V.L.B. de Jesus, B. Fischer, G. Gademann, K. Simeonidis, A. Achtelik, Th. Ergler, B. Feuerstein, C.D. Schröter, R. Moshammer, J. Ullrich, New Journal of Physics 10 (2008) 025007.
[39] Q. Tang, Y. Zhou, C. Huang, Q. Liao, P. Lu, Optics Express 17 (2012) 19580.
[40] A.S. Alnaser, D. Comtois, A.T. Hasan, D.M. Villeneuve, J.-C. Kieffer, I.V. Litvinyuk, Journal of Physics B 41 (2008) 031001.
[41] C. Cornaggia, Ph. Hering, Physical Review A 62 (2000) 023403.
[42] Y. Zhou, Q. Liao, P. Lu, Optics Express 18 (2010) 16025.
[43] S.L. Haan, Z.S. Smith, K.N. Shomsky, P.W. Plantinga, Journal of Physics B 42 (2009) 134009.
[44] Y. Zhou, Q. Liao, Q. Zhang, W. Hong, P. Lu, Optics Express 18 (2010) 632.
[45] J.S. Parker, B.J.S. Doherty, K.T. Taylor, K.D. Schultz, C.I. Blaga, L.F. DiMauro, Physical Review Letters 96 (2006) 133001.
[46] X. Wang, J.H. Eberly, New Journal of Physics 12 (2010) 093407.
[47] C. Huang, Y. Zhou, A.H. Tong, Q. Liao, W. Hong, P. Lu, Optics Express 19 (2011) 5627.
[48] Phay.J. Ho, R. Panfili, S.L. Haan, J.H. Eberly, Physical Review Letters 94 (2005) 093002.
[49] D.F. Ye, J. Chen, J. Liu, Physical Review A 77 (2008) 013403.